FLOMEKO 2003
11th IMEKO TC9 Conference on Flow Measurement
Groningen, NETHERLANDS, 12 - 14 May 2003

To be presented at FLOMEKO 2003
(paper reference number 001)

Modelling wet-gas annular-dispersed flow through a Venturi

M. van Werven[a], G. Ooms[b], B.J. Azzopardi[c], H.R.E. van Maanen[a]

(Accepted for publication in AIChE-Journal)

[a]Shell International Exploration and Production, Technical Applications and Research, P.O. Box 60, 2280 AB Rijswijk, The Netherlands
[b]J.M. Burgers Centre, Laboratory for Aero and Hydrodynamics, Delft University of Technology, Leeghwaterstraat 21, 2628 CJ Delft, The Netherlands
[c]Department of Chemical, Environmental and Mining Engineering, University of Nottingham, University Park, Nottingham NG7 2RD, UK

Abstract A theoretical model for gas-liquid annular-dispersed flow through a Venturi meter is reported. It is based on an earlier model developed for Venturi scrubbers. Changes implemented are based on new research and on the different physics between the two cases. The predictions of the model have been tested using information from recent experiments on Venturi meters employed for measuring wet gas flows with liquid volume fraction up to 10%. The model gives good predictions.

Keywords - Fluid mechanics, annular-dispersed multiphase flow, Venturi, deposition, entrainment,

1. INTRODUCTION

The convergent/divergent geometry commonly named after Giovanni Baptista **Venturi** has been widely used as a single-phase flow measurement device in pipelines, achieving a high accuracy and being simple and robust in design. The use of a Venturi meter to measure the flow rate of a liquid-solid flow (a flow of a liquid with particles) in a pipeline was first researched nearly forty years ago (Brook, 1962). Graf (1967) proposed, that the flow rates of both phases could be determined from the pressure drop to the throat and the overall pressure loss across the Venturi. Further work on this has been produced by Hirata *et al.* (1991, 1995).

The use of a Venturi as meter for a gas-liquid flow (a flow of a gas with liquid) in a pipeline has also been studied for a long time (Thompson *et al.*, 1966 and Harris, 1967). It is still a subject of research (Machado, 1997; Pinheiro da Silva Filho, 2000 and Hall *et al.*, 2000). Recent work has employed the Venturi, together with another independent measurement device, in order to determine the gas and liquid flow rates. However, to the best of our knowledge measurement of the gas and liquid flow rates in a pipeline with a Venturi only is still not generally possible.

Our plan is to develop a method to make such a measurement possible for so-called wet-gas flows, for which the mass flow rate of the liquid is not larger than that of the gas. As the liquid density is considerably higher than the gas density, the liquid volume fraction is not more that a few percent. Moreover the gas velocity is assumed to be high enough

for the flow pattern in the pipeline and in the Venturi to be annular/dispersed. The idea is to measure the pressure drop up to the Venturi throat and up to the end of the Venturi and to derive from these two measurements, using a theoretical model in inversion, the mass flow rates of the gas and the liquid.

For this it is essential to have an accurate theoretical model for annular-dispersed flow of a wet gas through a Venturi. To that purpose an existing theoretical model published in the open literature has been extended. This theoretical model was originally developed for describing the annular-dispersed gas-liquid flow in a Venturi scrubber, in order to predict the pressure drop across the Venturi and the collection efficiency for a gas cleaning application (Azzopardi *et al.*, 1991). The purpose of this paper is to report an extension of the original model, so that it can also be used for the measurement method of a gas-liquid annular-dispersed flow mentioned above.

In this paper, the new version of the model is presented. The predictions of a computer code incorporating the model are compared with experimental data obtained at high pressure with hydrocarbon fluids. Pressure drop to the Venturi throat, overall pressure loss and pressure profiles are considered. It will be shown that a good agreement exists between predictions made with the modified model and experimental data.

2. MODEL FOR ANNULAR-DISPERSED FLOW IN A VENTURI

The mathematical model that is used to describe the annular-dispersed flow through a Venturi consists of a one-dimensional model for the convergent section and throat section of the Venturi, and a quasi-one-dimensional model incorporating integral boundary layer description for the divergent section, Figure 1. The requirement for the more complex approach in the diffuser arises from the difference in sign of the pressure gradient that is present in these sections. In the convergent section and throat there is a favourable pressure gradient where pressure decreases with flow direction, the boundary layer becomes very thin and the flow can be assumed to have a uniform velocity distribution about the cross-section. In contrast, in the divergent section there is an unfavourable pressure gradient where the pressure increases with flow direction. From the start of the divergent section the flow is assumed to develop to a non-uniform profile with a significant growth of the boundary layer at the wall, which has been neglected in the one-dimensional model. In the convergent section, the throat and the divergent section a liquid film at the wall of the Venturi is assumed to be present.

2.1 One-dimensional model for the convergent section and the throat

A one-dimensional annular-dispersed model describes the gas-liquid flow in the first two sections (convergent section and throat). As mentioned a liquid film is assumed to be present at the wall. A dispersed phase of gas with droplets is present in the core region. So the presence of a very thin boundary layer at the gas-liquid interface is neglected. We will describe the flow quantitatively by a system of equations representing the mass and

momentum balances. With these equations we can solve the unknown variables (gas and droplet velocities, pressure) as a function of the axial co-ordinate of the Venturi.

Assuming we have *n* groups of droplets, the flow can be described by a system of *2n+2* equations; a mass conservation equation for the gas, *n* mass conservation equations for the droplets, *n* momentum conservation equations for the droplets and the pressure drop equation. With these equations we can solve *2n+2* variables; the core velocity of the gas, the mass flow rates and the velocities of the *n* different droplet groups and the pressure.

The mass conservation equation for the continuous gas phase is used in order to determine the gas velocity in the core at each axial position along the Venturi:

$$\frac{dW_G}{dx} = 0 \text{ , where } W_G = U_\infty r_G A. \qquad (1)$$

The velocity of the different groups of droplets (with different sizes) is determined by the drag force exerted by the gas on the droplets due to the velocity difference between gas and droplets. The following equations of motion are used to determine the velocities of the droplets in the different size groups:

$$U_{D_i} \frac{dU_{D_i}}{dx} = \frac{3}{4} C_{D_i} \left(\frac{r_G}{r_L} \right) \frac{\left| U_\infty - U_{D_i} \right| \left(U_\infty - U_{D_i} \right)}{d_{D_i}} \qquad (2)$$

where d_{D_i} is the mean droplet diameter of group *i*, calculated with the empirical correlation recommended by Azzopardi and Govan (1984):

$$d_{D_i} = l_T\left(\frac{15.4}{We^{'0.58}} + \frac{3.5\, r_G W_{LE}}{r_L W_G}\right) \tag{3}$$

where $l_T = \sqrt{\frac{s}{r_L g}}$ is the Taylor wavelength and $We' = \frac{r_L U_\infty^2 l_T}{s}$ is the Weber number. This droplet size equation accounts for break up from the film (1st term) and for coalescence (2nd term) (which particularly occurs at high liquid concentrations).

The drag coefficient is calculated with:

$$C_{D_i} = \begin{Bmatrix} \frac{24}{\mathrm{Re}_{D_i}}\left(1 + 0.15\,\mathrm{Re}_{D_i}\right)^{0.687} & for \quad \mathrm{Re}_{D_i} < 1000 \\ 0.44 & for \quad \mathrm{Re}_{D_i} \geq 1000 \end{Bmatrix} \tag{4}$$

where the droplets Reynolds number :

$$\mathrm{Re}_{D_i} = \frac{r_G \left|U_\infty - U_{D_i}\right| d_{D_i}}{m_G} \tag{5}$$

To determine the distribution of liquid between film and droplets we make use of mass transfer equations in order to calculate the entrainment rate E and deposition rate D per unit area of channel wall at each axial position along the Venturi:

$$\begin{aligned} E &= k_D C_E \\ D &= k_D C \end{aligned} \tag{5}$$

in which k_D is the mass transfer coefficient (dependent on the surface tension) calculated from the correlation of Whalley *et al.* (1974) and C_E is the equilibrium concentration of entrained droplets, calculated from the correlation of Whalley and Hewitt (1978).

In these diffusion equations, C is the actual mass concentration of droplets given by:

$$C = \sum_{i=1}^{n} \frac{W_{LE_i}}{AU_{D_i}} \tag{6}$$

Changes in mass flow rates of the liquid film and of the droplet groups (existing groups and the newly formed group) result from the entrainment and deposition rates at each position. The change in mass flow rate of the liquid film is given by:

$$\frac{dW_{LF}}{dx} = pd(D - E) \tag{7}$$

The mass flow rate of newly formed droplets is determined by:

$$\frac{dW_{LE_i}}{dx} = pdE \tag{8}$$

The Azzopardi-Govan relation determines the droplet diameter of the newly formed droplets. The change in mass flow rates of the existing droplet groups is given by:

$$\frac{dW_{LE_i}}{dx} = -pdD\frac{W_{LE_i}}{W_{LE}} \tag{9}$$

It has been observed that, in addition to the normal entrainment described by the above equations, there is additional entrainment which occurs at the boundary of the convergent and throat sections, Azzopardi and Govan (1984), Fernandez Alonso *et al.* (1999). A smaller effect has been found at the throat diffuser boundary, Leith *et al.* (1984). Fernandez Alonso et al. gathered data from experiments with different convergence angles and provided correlations for the limiting condition for this extra entrainment and for its magnitude their correlations had constants specific to each convergence angle. This information has been analysed further and a single correlation developed. This has the form

$$\Delta E_f = 1 - 1.063\left(\frac{We_c}{We}\right)^{0.34} \tag{10}$$

where, the critical Weber number for inception of extra entrainment is given by

$$We_c = 0.1857\left(90 - q/2\right) - 5.17 \tag{11}$$

with q being the angle of the convergence. Obviously, $\Delta E_f = 0$ for $We < We_c$.

So it is assumed, that the change in mass flow rate of an existing droplet group due to deposition is proportional to the mass flow rate of that particular group relative to the total mass flow rate of entrained liquid. The frictional effect of the flow are modelled through the shear stress at the interface between the gas-droplet core and the liquid film, and this stress is calculated through:

$$t_i = \frac{1}{2} f_i \left(r_G + C_h\right) U_{GC}^2 \tag{12}$$

Here, the interfacial friction factor is given by $f_i = f_{GC}\left(1 + 360\frac{m}{d}\right)$ as suggested by Wallis (1970). The gas and drops in the core are assumed to be travelling at the same velocity. The velocity of the mixture is given by:

$$U_{GC} = \frac{W_G}{Ar_G} + \frac{W_{LE}}{Ar_L} \tag{13}$$

where W_G and W_{LE} are the mass flow rates of gas and entrained liquid respectively and the contribution due to the droplets C_h is given by:

$$C_h = \frac{W_{LE}}{AU_{GC}} \tag{14}$$

The smooth wall friction factor f_{GC} is calculated by:

$$f_{GC} = \frac{0.079}{\mathrm{Re}_{GC}^{0.25}} \tag{15}$$

where the Reynolds number for the homogeneous core:

$$\mathrm{Re}_{GC} = \frac{(W_G + W_{LE})d}{Am_G} \tag{16}$$

The thickness of the liquid film m on the wall is derived by assuming that the ratio of the frictional pressure drop due to the film and the total frictional pressure drop is equal to the ratio of the liquid film cross-sectional area and the total cross-sectional area. The film thickness m is then calculated simultaneously with the interfacial shear stress using the (triangular) relationship:

$$m = \sqrt{\frac{\left(\frac{d}{4}\right)^3 \left(\frac{dp}{dx}\right)_{LF}}{t_i}} \tag{17}$$

where $(dp/dx)_{LF}$ is the frictional pressure derivative due to the liquid film, calculated by:

$$\left(\frac{dp}{dx}\right)_{LF} = \frac{2}{d} f_{LF} r_L U_{LF}^2 \tag{18}$$

This is the frictional pressure gradient that would occur, when the liquid in the film occupied the total cross section of the Venturi and flowed with cross-sectional averaged velocity. The liquid film friction factor is dependent on the liquid film Reynolds number:

$$f_{LF} = \left\{ \begin{array}{ll} \dfrac{16}{\mathrm{Re}_{LF}} & for \quad \mathrm{Re}_{LF} < 200 \\ \dfrac{0.079}{\mathrm{Re}_{LF}^{0.25}} & for \quad \mathrm{Re}_{LF} > 8000 \\ \dfrac{143.38}{(\ln \mathrm{Re}_{LF})^{4.5}} + 0.001069 & for \quad 200 \le \mathrm{Re}_{LF} \le 8000 \end{array} \right\} \tag{19}$$

and the liquid film Reynolds number is given by $\mathrm{Re}_{LF} = \frac{G_{LF} d}{m_L}$, where $G_{LF} = W_{LF}/A$ is the mass flux of the liquid film.

The momentum equation for the gas-droplet core is solved in order to calculate the pressure at the various positions along the Venturi. According to this equation the acceleration of the gas, the acceleration or deceleration term for the droplet groups (dependent on the relative velocity of the particular droplet group) and the friction at the interface between the core and the liquid film determine the pressure gradient. The pressure derivative is integrated with a fourth order Runge-Kutta subroutine.

$$-\frac{dp}{dx} = \frac{W_G}{A}\frac{dU_\infty}{dx} + \sum_{i=1}^{n}\frac{W_{LE_i}}{A}\frac{dU_{D_i}}{dx} + \frac{4t_i}{d} \qquad (20)$$

2.2 Boundary-layer model for the divergent section

In the divergent section of the Venturi a boundary-layer model is used to describe the flow, because of the unfavourable adverse pressure gradient that is present here. The flow in this section is divided in two regions: the core region and the boundary-layer region. In the core region the flow of gas and droplets is described as in the one-dimensional model. In the boundary-layer region it is assumed, that there are no droplets and the flow is modelled as a viscous flow over a rough surface. In the boundary-layer model we make use of a group of characteristic variables. These parameters are directly or indirectly dependent on the boundary layer thickness d, and are defined as:

the blockage parameter: $B = \frac{d^*}{R}$,

the blockage fraction: $\Lambda = \frac{d^*}{d}$,

the boundary layer shape factor: $H = \frac{d^*}{q}$,

and the shape factor: $h = \frac{H-1}{H}$.

In fact, by defining these parameters, we use two independent variables in the modelling; the displacement thickness d^* and the momentum thickness q.

2.2.1 Boundary layer region

The boundary layer region is quantitatively described by a system of equations consisting of a two-phase momentum integral equation (together with an assumed wall-wake velocity profile) and a boundary layer entrainment equation (together with a correlation for the boundary layer entrainment rate).

A momentum balance over the boundary layer region (in which the pressure at the edge of the boundary layer is taken into account) results in the following momentum integral equation:

$$\frac{dq}{dx} + (2+H)\frac{q}{U_\infty}\frac{dU_\infty}{dx} + \frac{q}{R}\frac{dR}{dx} + d\left(\frac{r_L}{r_G}\right)\frac{1}{U_\infty^2}\sum_{i=1}^{n} f_{D_i} U_{D_i}\frac{dU_{D_i}}{dx} = \frac{C_f}{2} \qquad (21)$$

in which ϕ_{Di} is the volume fraction of each group of drops, $C_f = k^2 V_T |V_T|$ is the skin friction coefficient and k is the Von Karman constant (= *0.41).* The non-dimensional shear velocity V_T (= $u_t/kU_¥$) obtained from integrating the fully rough form of the Coles wall-wake velocity profile over the boundary layer. This results in:

$$V_T = \frac{1-2\Lambda}{\ln\dfrac{\mathrm{Re}^*}{\Lambda} - \ln \mathrm{Re}_e + 1.485} \qquad (22)$$

The Reynolds number based on the displacement thickness d^* is defined as $\mathrm{Re}^* = U_\infty d^* / n$ and the Reynolds number based on the liquid film roughness is given by

$\mathrm{Re}_e = U_\infty e/n$. The roughness height is dependent on the thickness of the liquid film and is given by:

$$e = Km \tag{23}$$

The original value of K had been taken from publications on annular flow in vertical pipes. There, for wide ranges of flow rates, the interface is dominated by large, fast-moving structures usually called disturbance waves. These have been seen in Venturis at higher film flow rates. The height of these disturbance waves was five times the mean film thickness. A values of k = 5 was considered reasonable. In contrast, in both pipe flows and Venturis, when the film flow rates are low, there are no disturbance waves and the interface is covered by ripples of much lower amplitude and celerity. A much lower value of K is needed. In the present work a value of 0.085 was chosen.

A mass balance over the boundary layer region gives us the boundary layer entrainment equation:

$$\frac{1}{RU_\infty}\frac{d}{dx}\left[RU_\infty\left(d-d^*\right)\right]=E_b \tag{24}$$

E_b is the dimensionless boundary layer entrainment rate, which is determined from the correlation suggested by Ferziger *et al.* (1982), i.e.,

$$E_b = 0.0083\left(1-\Lambda\right)^{-2.5} \tag{25}$$

2.2.2 Core region

In the core region we have the continuity equation, *dQ/dx = 0*, where the cross section of flow surface is reduced due to the presence of the boundary layer. The volumetric flow rate, in which the volume fraction of the droplets has been neglected, is given by:

$$Q = U_\infty \pi R^2 (1-B)^2 = U_\infty \pi \left(R - d^*\right)^2 \tag{26}$$

Using this flow rate equation, the mass continuity equation can be written as:

$$\frac{1}{U_\infty}\frac{dU_\infty}{dx} = \frac{2}{1-B}\frac{dB}{dx} - \frac{2}{R}\frac{dR}{dx} \tag{27}$$

The pressure is calculated as in the convergent section and throat (taking into account again the deposition, entrainment, and acceleration or deceleration of the droplets).

2.3 Calculation procedure

The model consists of a number of ordinary differential equations. They have been incorporated into a Fortran computer programme and integrated along the Venturi from initial values using a 4th order Runge-Kutta-Merson numerical procedure. For this particular application it is important to know how much liquid is travelling as drops at the entrance of the Venturi and what is the size of those drops. The method used for these parameters are discussed below.

3. EXPERIMENTAL DATA

Two sets of experimental data have been used to test the model described in section 2. The first was obtained at the wet-gas test facility of CEESI in Colorado, USA. The venturi was installed in a 0.097 m diameter pipe and had a 0.058 m diameter throat one diameter long. The convergence and diffuser angles were 30° and 7° respectively. The

fluids employed were methane and decane. The ranges of pressures, gas upstream velocities and liquid loading are given in Table 1.

Table 1: Ranges of parameters used in experiments

P (bar)	***U_g (m/s)***	***Liquid loading (W_L/W_G) (%)***
14	3 - 12	0 - 50
48	3 - 12	0 - 50
83	3 - 12	0 - 50

The fraction of liquid in the flow (the so-called wetness of the gas) is often expressed by the Lockhart-Martinelli parameter *X*. For the CEESI data-set, *X* ranges from 0 to 0.15

The second set of data was obtained at the SINTEF facility in Norway. Here the Venturi was installed in a 0.097 m diameter pipe and had a 0.039 m diameter throat approximately one diameter long. The convergence and diffuser angles were 21.5° and 7.65° respectively. Pressures in the range 15-90 bar, gas upstream velocities of 7-12 m/s and liquid loadings up to 81% by mass were used. The fluids employed were nitrogen and diesel.

4. SENSITIVITY OF MODEL

Before testing the model against the experimental data described in Section 3, tests were carried out to establish the sensitivity of the model. A first test considered the simplification of ignoring the boundary layer in the convergence and throat sections on

the grounds that it would be thin enough to be negligible. This was tested using a second computer programme which used the boundary layer model all along the Venturi. Figure 2 shows the predicted boundary layer thickness, as dimensionless momentum thickness, for both cases. As can be seen, the boundary layer is indeed negligibly thin and both models give equivalent boundary layer growth in the diffuser. Figure 3, which presents the pressure difference along the Venturi, again shows no difference between the two predictions.

The effect of the values of the initial conditions of the boundary layer parameters, B_o and $\Lambda_{o,}$ were considered in the second test of sensitivity. Figure 4 shows the result of one such test and illustrates the lack of sensitivity to these parameters.

The third test concerns the initial distribution of liquid between film and drops. Here calculations have been carried out for two extreme cases, entrained fraction = 0 and =1. Runs were carried out at a typical liquid loading (25% liquid to gas by mass) and for one greater than the usual scope of wet gas meters (100% liquid to gas by mass). Figure 5 shows the variation of entrained fraction along the Venturi whilst Figure 6 illustrates the pressure difference profiles. The results indicate that, for the all-drops cases, little deposition occurs. When the liquid is introduced as a film, there is a continuous increase in entrained fraction with a very noticeable step change at the start of the throat. The effect initial entrained fraction is also clearly visible in the pressure difference profile. Pressure differences are higher for all the flow entering as a film because the newly created drops has to be accelerated over a greater difference in velocity. These results

should be considered in the context of entrained fractions expected in gas production fields. Though there is a considerable literature on entrained fraction in vertical upwards flow, data for horizontal pipes are more limited. Moreover, they tend to be confined to air/water flows. An exception to this is found in the work of Hoogerndoorn and Welling (1965) who used pipes upto 0.1 m diameter and employed low surface tension liquids. The correlation they propose suggests that entrained fractions will be 1.0.

The effect of the initial drops size has also been considered. The equation suggested by Azzopardi and Govan (1984), equation (3), was originally derived from data from upwards annular flow in vertical pipes. The data had been taken in pipe of 0.01-0.127 m diameter. The fluids were mainly air/water though both surface tension and gas density were tested in the smallest diameter pipe. Recent data from air/water experiments in a 0.095 m diameter horizontal pipe, Simmons and Hanratty (2001), has permitted a further test of equation (3). Here the predictions were within 0% to -33% of the measured values. To cover a slightly greater range calculations were carried out with drop sizes equal to and ±50% of the values given by equation (3). The results are presented in Figure 7 where an effect of drop size can be seen. However, the effect is not as great as the drop size variation with errors of +13.3% to –8.1% for the pressure drop to the throat and +14.6% to –11.5% for the total pressure drop across the Venturi.

5. COMPARISONS BETWEEN MODEL PREDICTIONS AND EXPERIMENTAL DATA

Comparisons were made between the experimental data and predictions made with the theoretical model described in the preceding section. The data used for the comparison were chosen in such a way, that they cover the full ranges of parameters varied in the experiments. Initial comparisons were made for single-phase flow. Figure 8 shows good agreement with experimental data for both pressure drop to the Venturi throat and overall pressure drop. Also shown is the value of the mechanical energy which characterised Bernoulli's law. Only a small variation in the mechanical energy is seen (about 4%). This is due to the variation of the density along the Venturi.

From the sensitivity results shown in Figure 4, inlet values of the boundary layer parameters B and L were set to 10^{-4}, 10^{-3} respectively. The model is shown to predict both single-phase and two-phase data successfully, Figure 9. Similar agreement was found over the ranges of pressures, gas flow rates and liquid loading that were used in the experiments.

Attention was given to the possibility of separation (or sometimes called detachment) of the boundary layer. Although the theoretical model is capable of dealing with separation of the boundary layer in the divergent section, numerical problems arise when separation really occurs. However, no separation of the boundary layer is obtained for the conditions in this work.

The split of liquid between film and drops can be expressed through the entrained fraction. Figure 10 shows a comparison between total pressure drops measured at CEESI and predictions made with the modified model as function of the liquid load for two initial values of the entrained liquid fraction at the start of the Venturi. Values are shown for all liquid initially travelling as film or all as drops. It can be seen that the total pressure drops show an almost linear relationship with the liquid load (for high values of the liquid loads). The pressure drop is higher for the initially low entrainment case because here the film flow rate is higher, above the critical value for the occurrence of disturbance waves and thence the roughness/film thickness ratio takes the higher value.

Figures 11 and 12 reveal that predictions of pressure drop (made with the modified model) are in good agreement with experiments when the experiments were in annular-dispersed flow. Predictions made for experiments from stratified-wavy flow were poorer. This can be expected, as the model is based on the assumption of annular-dispersed flow. The determination of the flow regime is based on the method taken from Oliemans (1998).

The model also gave good predictions of the experimental results obtained at the SINTEF facility. Figures 13 and 14 show comparisons, at 15 and 90 bar. Again good agreement is obtained and shows that the effect of a different geometry and a different fluids pair, nitrogen-Diesel oil instead of methane-decane, can be handled. The SINTEF data set covers four different line pressures. Good agreement was obtained over the ranges of pressures.

6. CONCLUSIONS

1. For annular-dispersed flow the modified model is in good agreement with the CEESI data and the SINTEF data.

2. The range of applicability of the model seems promising, since application of the modified model to completely different experiments (different Venturi geometry and different fluid pairs in the SINTEF experiments compared to the CEESI experiments) gives good predictions for all cases.

3. Further work is required to determine how the model can be adapted to the stratified-wavy flow pattern.

NOTATION

A	Cross section surface area	m^2
B	Boundary layer parameter	-
C	Droplet concentration	kg/m^3
C_D	Drag coefficient	-
C_E	Equilibrium concentration	kg/m^3
C_f	Skin friction factor	-
C_h	Homogeneous droplet concentration	kg/m^3
d	Local diameter	m
d_D	Droplet diameter	m
D	Deposition rate	kg/m^2s
E	Entrainment rate	kg/m^2s
E_b	Boundary layer entrainment rate	-
E_f	Entrained fraction	-
f	Fanning friction factor	-
g	Gravitational acceleration	m/s^2
G	Mass flux	kg/m^2s
h	Shape factor	-
H	Boundary layer shape factor	-
k	Von Karman constant (= 0.41)	-
k_D	Mass transfer coefficient	m/s
m	Thickness of liquid film	m
n	Total number of droplet groups	-
p	Local pressure	kg/ms^2
dp/dx	Local pressure derivative	kg/m^2s^2
$(dp/dx)_{LF}$	Frictional pressure gradient due to the liquid film	kg/m^2s^2
Q	Volume flow rate	m^3/s
R	Local radius	m
Re	Reynolds number	-
Re_D	Droplet Reynolds number	-
Re_{GC}	Homogeneous core Reynolds number	-
Re_{LF}	Liquid film Reynolds number	-
Re_e	Reynolds number based on liquid film roughness	-
Re^*	Reynolds number based on displacement thickness	-
U	Local velocity	m/s
$U_¥$	Core velocity	m/s
W	Mass flow rate	kg/s
We'	Weber number	-
x	Axial distance	m
X	Lockhart-Martinelli parameter	-

Greek symbols

d	Boundary layer thickness	m
d^*	Displacement thickness	m
e	Liquid film mean roughness height	m
l_T	Taylor wavelength	m
L	Boundary layer blockage fraction	-
m	Viscosity	kg/ms
n	Kinematic viscosity	m^2/s
q	Momentum thickness	m
r	Density	kg/m
s	Surface tension	kg/s
t_I	Interfacial shear stress	kg/ms^2

Subscripts

D	Droplet
G	Gas
GC	Homogeneous annular flow core
I	Group of droplet
L	Liquid
LE	Entrained liquid in the core region
LF	Liquid film at the Venturi wall
¥	Core

REFERENCES

Azzopardi, B.J. and Govan, A.H. (1984) The modelling of venturi scrubbers. *Filtration and Separation* **21**, 196-200.

Azzopardi, B.J., Teixeira, S.F.C.F., Govan, A.H. and Bott, T.R. (1991) An improved model for pressure drop in Venturi scrubbers. *Trans. I. Chem. E.* **69B**, 237-245.

Brook, N. (1962) Flow measurement of solid-liquid mixtures using venturi and other meters. *Proc. I. Mech. E.*, **176**, 127-140.

Fernandez Alonso, D., Azzopardi, B.J. and Hills, J.H. (1999) Gas/liquid flow in laboratory-scale venturis. *Trans. I. Chem. E*, **77B**, 205-211.

Ferziger, J.H., Lyrio, A.A. and Bardina, J.G. (1982) New skin friction and entrainment correlations for turbulent boundary layers. *Trans. A.S.M.E., J. Fluids Eng.*, **104**, 537-540.

Graf, W.H. (1967) A modified venturimeter for measuring two-phase flow. *J. Hydraulic Res.*, **5**, 161-187.

Hall, A.R.W., Reader-Harris, M.J. and Millington, B.C. (2000) A study of the performance of Venturi meters in multiphase flow. 2nd North American Conference on Multiphase Technology, Banff, Canada, 21 - 23 June 2000.

Harris, D.M. (1967) Calibration of a steam quality meter for channel power measurement in the prototype S.G.H.W Reactor. European Two-Phase Flow Group Meeting, Bournmouth.

Hirata, Y, Takano, M. and Narasaka, T. (1991) Measurements of flow rates and particle concentrations in heterogeneous solid-water two-phase flows by means of a Venturi. *JSME Int. J.*, **34B**, 304-309.

Hirata, Y, Takano, M. and Narasaka, T. (1995) Simultaneous measurements of flow rates and particle concentrations in heterogeneous solid-water two-phase flows by means of one Venturi. *JSME Int. J.*, **38B**, 440-447.

Hoogerndoorn, C.J. and Welling, W.A. (1965) Experimental studies on the characxteristics of annular mist flow in horizontal pipes. Symposium on Two Phase Flow, Exeter, 21-23 June, Paper C3.

Leith D., Martin K.P. and Cooper D.W. (1985) Liquid utilisation in a Venturi scrubber, *Filtration and Separation*, 21, 191-195.

Machado, R.T.M. (1997) Multiphase flow in a Venturi: an experimental and theoretical study. PhD Thesis, Imperial College, London.

Oliemans, R.V.A. (1998) Applied Multiphase Flow. Lecture notes. Department of Applied Physics, Delft University of Technology.

Pinheiro da Silva Filho, J.A. (2000) DIC Thesis, Imperial College, London.

Simmons, M.J.H. and Hanratty T.J. (2001) Droplet size measurements in horizontal annular gas-liquid flow. Int. J. Multiphase Flow, 27, 861-883.

Thomson, J.G., Hacking, H. and Cuthbertson, M.G. (1966) S.G.H.W.R. steam meter calibration trails. BSRA Marine Engineering Contract Report No. W.46.

Wallis, G.B. (1970) Annular two-phase flow: Part 2 Additional effects. J. Basic Eng., vol. 92, pp 73 82.

Whalley, P.B., Hutchinson, P. and Hewitt, G.F. (1974) The calculation of critical heat flux in forced convection boiling. *Heat Transfer 1974*, Scripta Book Co., **4**, 290-294.

Whalley, P.B. and Hewitt, G.F. (1978) The correlation of liquid entrainment rate in annular two-phase flow. UKAEA Report AERE R-9187.

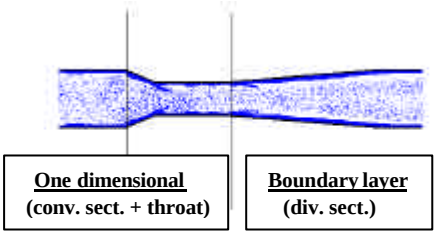

Figure 1 Venturi geometry and models used

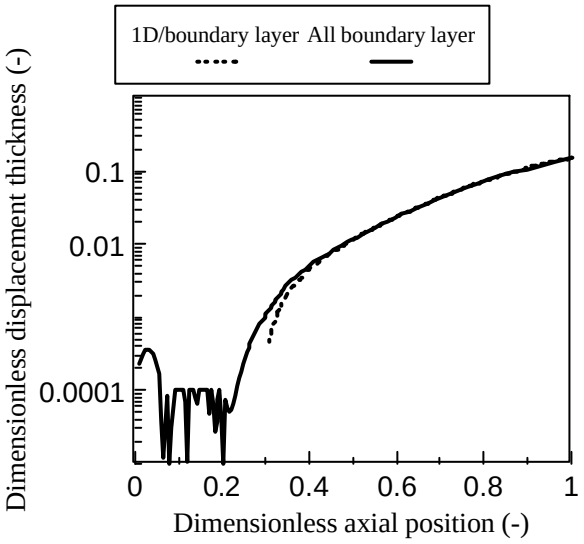

Figure 2 Axial distribution of dimensionless displacement thickness showing agreement between the one dimensional/boundary layer model and the all boundary layer model

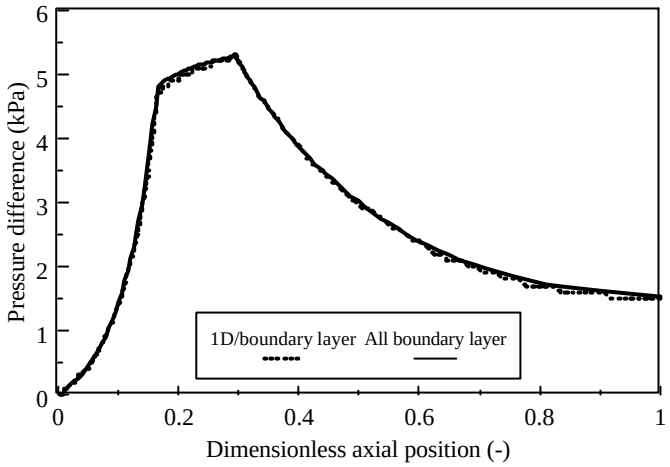

Figure3 Axial pressure profiles showing agreement between one dimensional/boundary layer model and all boundary layer model

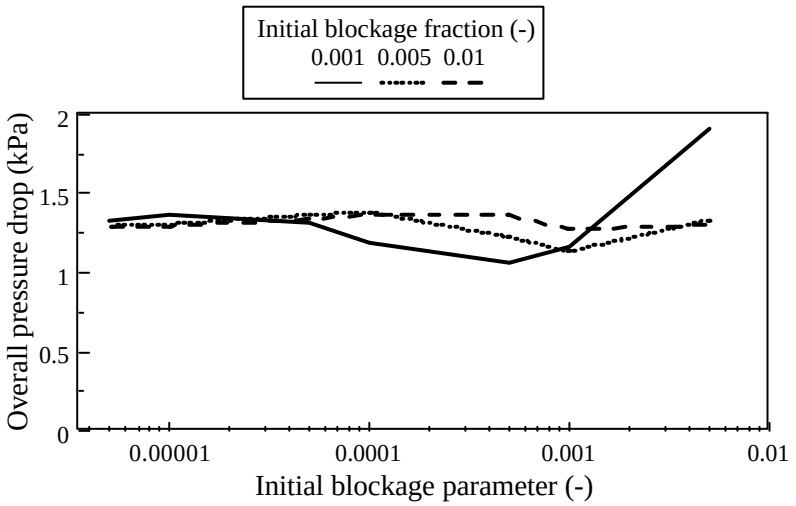

Figure 4 Effect of initial boundary layer parameters on overall pressure drop

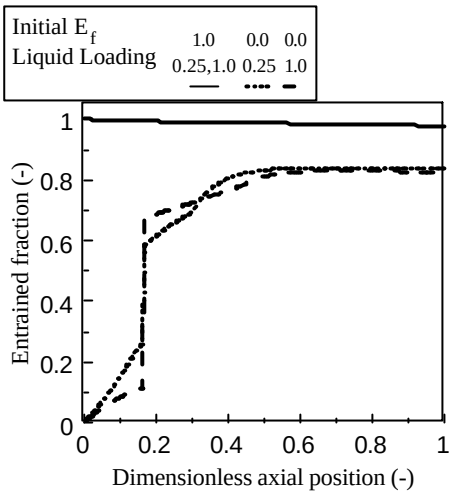

Figure 5 Axial variation of entrained fraction showing effect of initial entrained fraction and of liquid loading

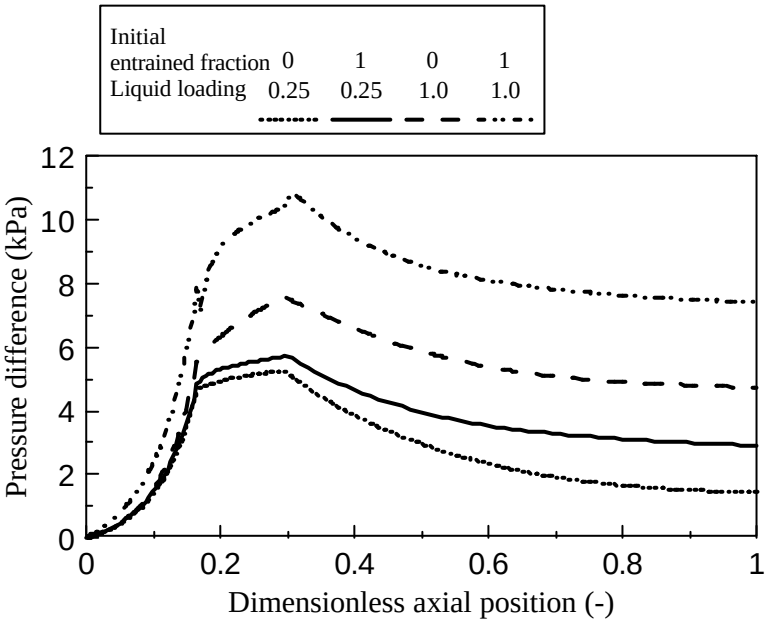

Figure 6 Axial variation of pressure difference showing effect of initial entrained fraction and of liquid loading

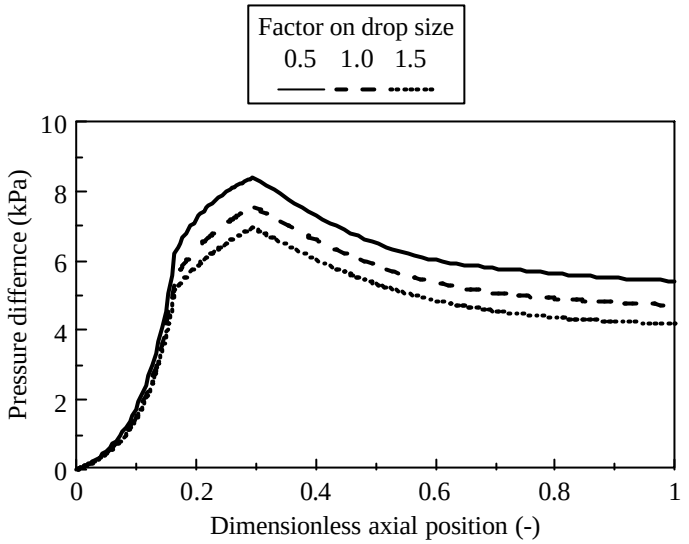

Figure 7 Effect of initial drop size on pressure difference profile.

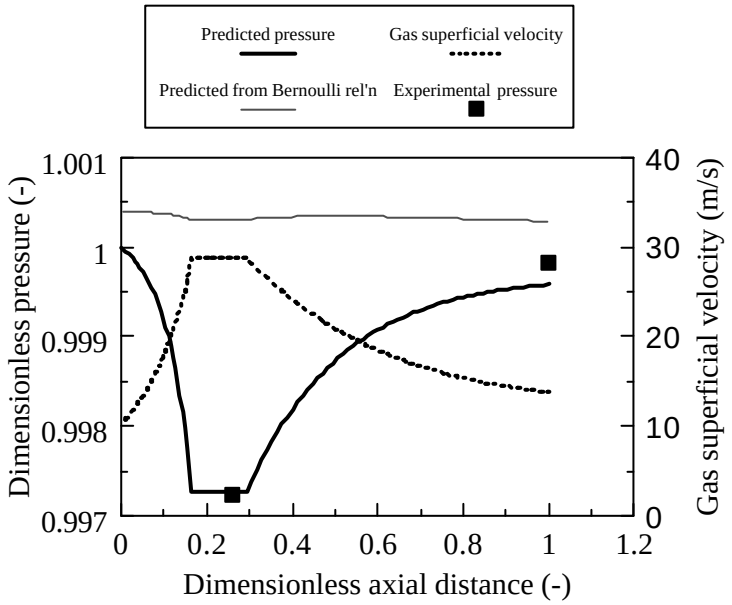

Figure 8. Pressure profile, velocity variation and Bernoulli's constant for single phase flow without viscosity

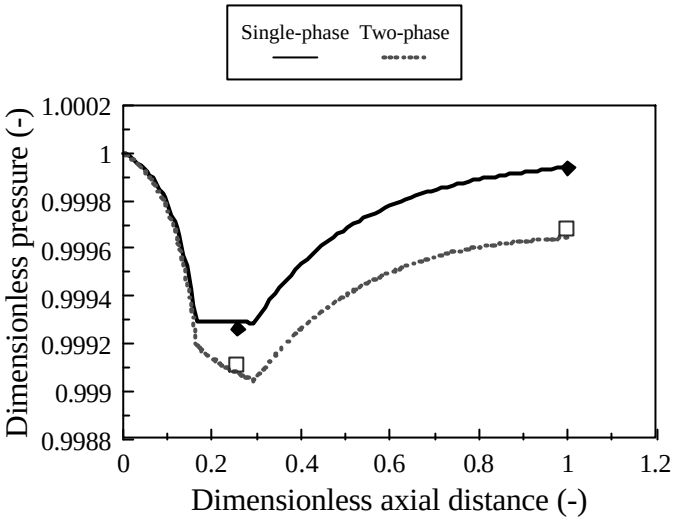

Figure 9 Predictions of pressure profiles compared to experimental data.

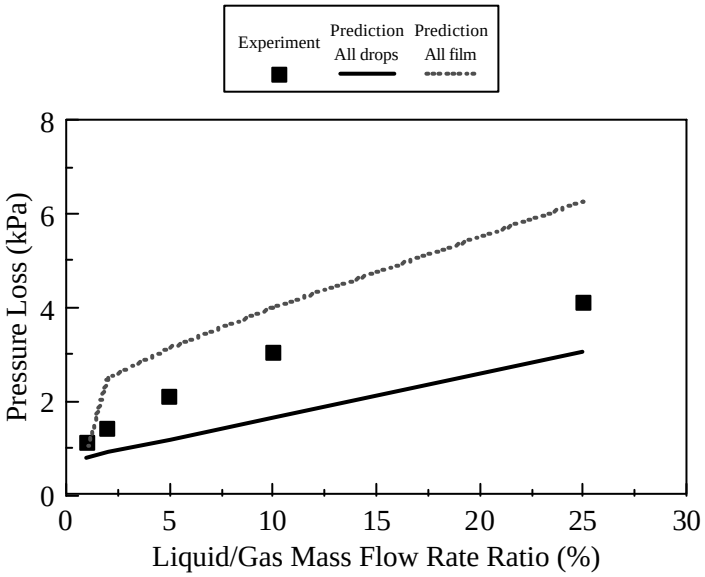

Figure 10 Recovery differential pressures against liquid loading for the extreme inlet values of the entrained fraction.

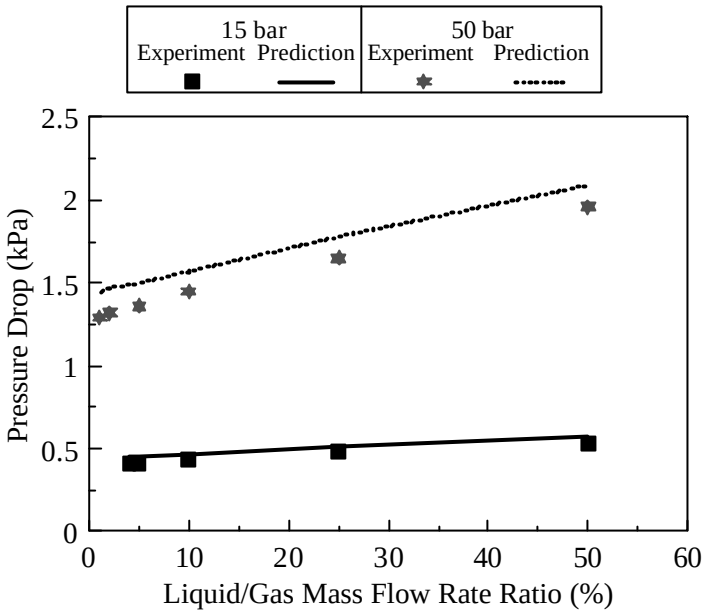

Figure11 Venturi differential pressures as function of liquid loading for stratified-wavy flow

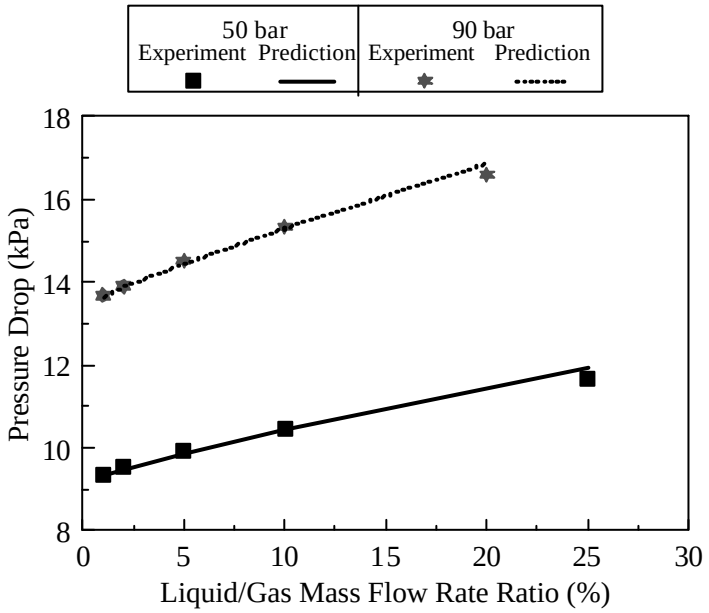

Figure12 Venturi differential pressures against liquid loading for annular-dispersed flow

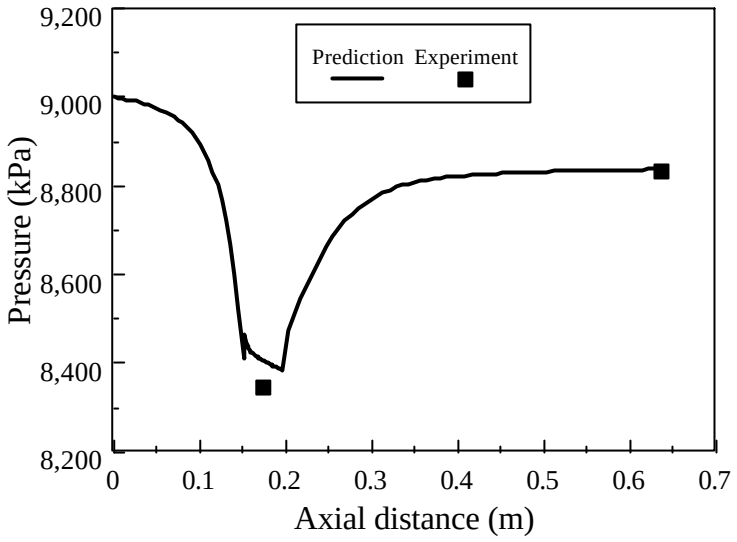

Figure 13 Pressure prediction with the modified model compared to SINTEF data, 90 bar

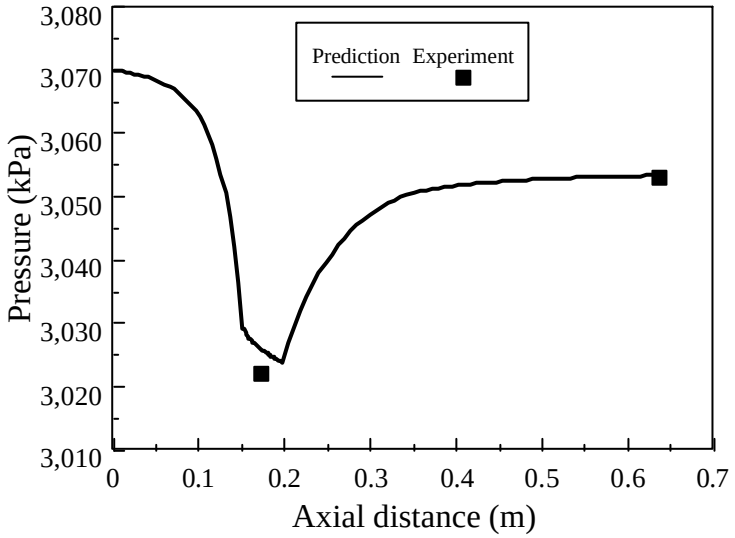

Figure 14 Pressure prediction with the modified model compared to SINTEF data, 30 bar